energies

MDPI

Article

Enhancing Thermal–Hydraulic Performance in Nuclear Reactor Subchannels with Al_2O_3 Nanofluids: A CFD Analysis

Mohammad A. I. Sardar *, Mushfiqur Rahman and Philip Rubini

School of Engineering, University of Hull, Hull HU6 7RX, UK; mushfiqur.rahman707@gmail.com (M.R.); p.a.rubini@hull.ac.uk (P.R.)

* Correspondence: imran.nse2@gmail.com; Tel.: +44-(0)-7845928527

Abstract: In this paper, the performance of aluminum-based nanofluids with a possible application in pressurized water reactors is numerically investigated. A 605 mm long 4-rod array square (2 × 2) subchannel geometry with a uniform heat flux of 50 kW/m^2 has been used in CFD simulation. This analysis has been carried out using the RNG k-epsilon turbulence model with standard wall function in ANSYS FLUENT 2022R1. The impact of various flow conditions and nanofluid concentrations has been examined. The effects of variable velocities on nanofluid performance have been studied using different Reynolds numbers of 20,000, 40,000, 60,000, and 80,000. The analysis was conducted with Al_2O_3/water nanofluid concentrations of 1%, 2%, 3%, and 4%. A comparison of the Nusselt number based on five different correlations was conducted, and deviations from each correlation were then presented. The homogeneous single-phase mixer approach has been adopted to model nanofluid characteristics. The result shows a gradual enhancement in the heat transfer coefficient with increasing volume concentrations and Reynolds numbers. A maximum heat transfer coefficient has been calculated for nanofluid at maximum volume concentrations (ϕ = 4%) and highest velocities (Re = 80,000). Compared to the base fluid, heat transfer was enhanced by a factor of 1.09 using 4% Al_2O_3. The Nusselt number was calculated with a minimal error of 3.62% when compared to the Presser correlation and the maximum deviation has been found from the Dittus–Boelter correlation (13.77%). Overall, the findings suggest that aluminum-based nanofluids could offer enhanced heat transfer capabilities in pressurized water reactors.

Keywords: nanofluid; base fluid; ANSYS; numerical analysis; heat transfer; Al_2O_3; Reynolds number; Nusselt number; pressurized water reactor; heat transfer coefficient

Citation: Sardar, M.A.I.; Rahman, M.; Rubini, P. Enhancing Thermal–Hydraulic Performance in Nuclear Reactor Subchannels with Al_2O_3 Nanofluids: A CFD Analysis. *Energies* **2024**, *17*, 5486. https://doi.org/10.3390/en17215486

Academic Editors: Tadeusz Bohdal and Marcin Kruzel

Received: 13 June 2024
Revised: 19 October 2024
Accepted: 25 October 2024
Published: 1 November 2024

1. Introduction

The main limitation of conventional fluids is their low thermal conductivity, which makes them less suitable for many industrial applications. In engineering, efficient cooling and heating processes are crucial for the safety and performance of thermodynamic systems. Specifically, the safety of nuclear power plants depends on the ability to effectively cool the reactor core to prevent overheating and potential accidents. Nuclear reactors are devices that utilize controlled nuclear fission to produce thermal energy for power generation [1]. Enhancing convective heat transfer (CHT) between the fuel rods and the coolant in nuclear reactors is, therefore, essential [2,3]. Given the direct link between nuclear plant safety and global energy security, continuous improvements in nuclear energy safety are paramount. The International Atomic Energy Agency (IAEA) emphasizes making nuclear energy rational, sustainable, and safe. As the number of nuclear power plants increases worldwide, ensuring their safety remains a major concern. The coolant in nuclear reactors is responsible for extracting heat from the fuel to ensure safe and cost-effective operation [4]. Maintaining sufficient coolant flow through the fuel channel is crucial to absorb excessive heat from the fuel rods. Subchannel analysis, such as investigating heat transfer performance in reactor rod bundle configurations, is popular due to its simplicity and effectiveness [4].

Figure 1 depicts a square subchannel in a 2 × 2 array of a nuclear reactor fuel assembly, but investigations can be carried out using other shapes and arrays [1].

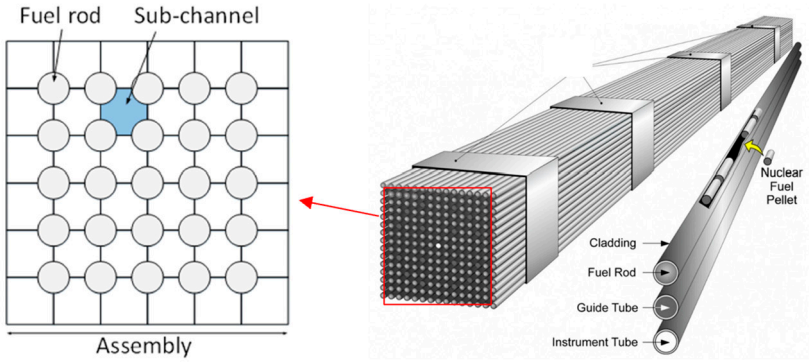

Figure 1. Nuclear reactor fuel rod subchannel [5].

Improving the heat transfer efficiency of a system is both important and challenging. Several methods have been proposed to enhance heat transfer performance, including surface treatments, flow perturbations, and the modifications of the flow structure using grid spacers, mixing vanes, and wire-wrapped rods [6]. However, due to manufacturing limitations, costs, and regulatory constraints, modifying the geometries of nuclear rod bundles is not straightforward. Alternatively, conductive heat transfer can be increased by using fluids with enhanced heat transfer characteristics [7–9]. The use of suspended nanoparticles (1~100 nm) in base fluid is one of them [10]. The distinguishing characteristics of nanofluids include a considerable rise in liquid viscosity, thermal conductivity, and heat transfer coefficient. In solid form, metals have a higher thermal conductivity than fluids at room temperature [11]. A metal like copper, aluminum, or gold conducts heat more effectively than a fluid like water, oil, or ethylene glycol and water mixed. Copper and aluminum, for example, conduct heat 665 and 400 times better than water. Therefore, fluids containing suspended metal particles should have higher thermal conductivities than pure fluids because metallic liquids have a much greater thermal conductivity than non-metallic liquids. The other reasons behind the enhanced thermal conductivity and heat transfer coefficient of nanofluids are the diffusion of the suspended particles, increased relative surface area of the fluid [12], intensification of turbulence, Brownian motion [13,14] thermophoresis, and diffusiophoresis [15]. Since the heat transfer rate of nanofluids is high and their thermal conductivity is better than that of base fluids, applying nanofluids can be carried out with smaller-sized equipment [16]. Despite the fact that modified coolants such as a base fluid with suspended nanoparticles can enhance the thermal–hydraulic performance of reactor rod bundles, this would necessitate a thorough investigation.

Recent advancements in nanofluid research have demonstrated significant improvements in thermal and physical properties, particularly with the development of hybrid nanofluids. However, challenges such as maintaining stability, complex preparation methods, high costs, and potential health and environmental concerns persist [17]. Innovative approaches, including the use of hybrid and green nanofluids, as well as advanced characterization techniques, are being explored to address these issues [18]. Recent studies have also focused on the use of nanofluids demonstrating their potential to optimize processes, improve tool life, and enhance thermal performance in the last 5 years [19,20].

Khalid et al. [21] investigated the use of nanofluids to improve heat transfer in nuclear reactors with four different nanofluids—Al_2O_3–H_2O, ZrO_2–H_2O, Ag–H_2O, and Si–H_2O—using CFD in a high-power area of an HPR-1000 reactor. The silver–water (Ag–H_2O) nanofluid showed the best performance, with a 67.15% increase in heat transfer coefficient (HTC) and a 45.23% improvement in the minimum departure from nucleate boiling ratio (MDNBR) compared to pure water. It also reduced the fuel rod wall temperature by 28.5 K. They also found that higher concentrations of nanofluids resulted in increased outlet temperatures and required less coolant flow, potentially leading to smaller reactor

designs. At the highest concentration, the fuel rod cladding stayed cooler, improving the reactor's safety margin. Overall, they concluded that silver–water nanofluid offers significant potential to enhance reactor safety and efficiency.

Uzun [22] studied the use of magnesium oxide (MgO) and zinc oxide nanoparticles to improve heat transfer in VVER-1000 nuclear reactors by adding them to the reactor coolant to enhance its thermal properties. With the addition of 0.2% MgO nanoparticles, the coolant temperature increased to 617.4 K compared to 613.7 K for standard light water. The use of nanoparticles also improved the enthalpy value, reaching 1303.6 kJ/kg at the end of the channel. Overall, the research demonstrates that adding nanoparticles to the coolant improves heat transfer efficiency, leading to higher coolant temperatures and better thermal performance in nuclear reactors.

Ponkty et al. [23] used COMSOL to study reactor passive heat removal system and found that Passive Residual Heat Removal Heat Exchangers (PRHR HXs) with C-tube bundles improve emergency cooling, while flower baffles in heat exchangers increase efficiency and reduce flow friction. Their study focusses on optimizing reactor safety and reliability.

Khouri et al. [24] explored the advantages and challenges of flow boiling using both pure liquids and nanofluids in microchannel heat sinks. They tested various nanoparticle concentrations and found that even minimal concentrations of Au nanofluids provided superior cooling performance. The study concluded that nanoparticles could significantly enhance heat transfer, offering a cost-effective alternative to traditional two-phase flow approaches.

Zhuang et al. [25] experimentally examined flow boiling heat transfer and pressure drop in microchannels with a pin-fin array, proposing improved correlations for pressure drop and heat transfer coefficients. Similarly, Ghafouri and Toghraie [26] explored the thermal conductivity of SiC-ZnO/ethylene glycol hybrid nanofluid, showing enhancements with smaller nanoparticle sizes, higher temperatures, and larger volume fractions, and formulated an optimized multivariate correlation. This research complements these studies by investigating heat transfer mechanisms in microchannel systems, with a focus on validating results against the established correlations like those proposed by Zhuang et al. [25] and Ghafouri and Toghraie [26]. The findings contribute to enhancing predictive models for nanofluid applications in microchannel heat transfer systems. In another study, Marseglia et al. [27] evaluated the thermal performance of water-based GO nanofluids in a heat exchanger, highlighting how increased nanoparticle concentration and temperature improved thermal conductivity and convective heat transfer. They developed a new correlation for predicting the Nusselt number in nanofluids, emphasizing the potential of these fluids to enhance industrial heat exchangers' performance.

Shojib et al. [28] explore the use of nanofluids as a primary coolant in pressurized water reactors (PWRs) to improve heat transfer and prevent core meltdown. They found that a 1–4% increase in nanoparticle concentration can significantly enhance heat transfer, potentially allowing for substantial power upgrades without altering fuel assembly design.

Khashaei et al. [29] investigated Al_2O_3 nanofluids in deep dimpled tubes under laminar flow conditions. Their research demonstrated significant heat transfer improvements due to vortex generation and enhanced flow mixing. The deep dimpled tubes showed a 3.42-fold increase in the convective heat transfer coefficient, offering a highly efficient solution for heat exchanger applications.

Alshukri et al. [30] examined the thermal–hydraulic performance of a baffled channel with three different nanofluids—water-SiO_2, water-Al_2O_3, and water-CuO—compared to pure water. The channel features staggered rectangular baffles at varying inclination angles (0°, ±10°) across Reynolds numbers from 5000 to 50,000. Numerical simulations were conducted using ANSYS Fluent, and the results were validated with experimental data. The research shows that nanofluids, especially water-CuO, enhance heat transfer, with a 10.3% increase in the heat transfer coefficient compared to pure water. However, using nanofluids also led to a higher pressure drop than pure water. Overall, the study

reveals that nanofluids improve heat transfer performance, particularly water-CuO, but come with increased pressure drop and friction compared to pure water.

Computational Fluid Dynamics (CFD) is a powerful tool that uses numerical methods to analyze fluid flow by solving complex equations that govern fluid behavior. It allows scientists and engineers to simulate real-world fluid dynamics on computers, making it a cost-effective and efficient alternative to physical experiments, which can be expensive, time-consuming, or impractical. CFD works based on fundamental principles like mass, momentum, and energy conservation. It is widely used in industries such as aerospace, automotive, energy, and environmental engineering. In the energy sector, particularly in nuclear engineering, CFD plays a key role in analyzing how coolants flow in reactor fuel rod bundles. This is critical for reactor safety and performance. CFD is an advanced and rapidly evolving field that employs numerical methods and algorithms to solve complex problems involving fluid flow.

In the energy sector, and particularly in nuclear engineering, CFD has become an indispensable tool for analyzing fluid flows under extreme conditions, such as the turbulent flow of coolants in reactor fuel rod bundles. These systems are crucial for reactor efficiency and safety, but their complexity makes experimental analysis difficult, especially when dealing with nanofluid turbulent convection [31,32]. CFD offers a detailed, reliable, and cost-effective way to study these challenging conditions, providing insights that are otherwise hard to obtain through physical testing.

Among the many CFD software tools, ANSYS Fluent is one of the most recognized due to its advanced modeling capabilities and widespread acceptance in industries ranging from energy to aerospace. Fluent excels in simulating fluid flow in highly complex geometries, handling turbulence, and modeling multiphase systems with remarkable precision [33]. These capabilities make it particularly well suited for simulating fluid dynamics in nuclear reactor subchannels, where intricate flow patterns, heat transfer mechanisms, and safety-critical systems come into play. The ability to accurately model these systems using Fluent is crucial for optimizing reactor performance, ensuring safety, and driving innovation in nuclear and other high-stakes engineering fields.

This paper builds upon these capabilities by investigating the thermal–hydraulic performance of an Al_2O_3/water nanofluid in a nuclear reactor fuel rod bundle subchannel using ANSYS Fluent. The study employs a 3D double-precision parallel steady-state solver, and its results contribute significantly to the theory of turbulent convection in nanofluids. By examining the flow of Al_2O_3/water nanofluid at various Reynolds numbers (20,000 to 80,000) and volume concentrations (1–4%), this research not only validates the effectiveness of nanofluids in enhancing heat transfer but also offers critical insights into their practical applications in reactor safety. The findings demonstrate a notable improvement in the heat transfer coefficient, reinforcing the potential of nanofluids to optimize nuclear reactor cooling systems.

2. Materials and Methods

2.1. Nanofluid Hest Transfer Modelling

To apply nanofluid in real life, it is important and essential to model its heat transfer behavior. There are several heat transfer models for nanofluid available, for instance, the dispersion model, particle migration model, and single-phase and two-phase models.

In this study, the single-phase model is employed to conserve computational resources, treating the nanofluid as behaving similarly to a conventional single-phase fluid. Nanofluids behave like single-phase fluids because the nanoparticles are extremely small and evenly dispersed, resulting in a homogeneous mixture. Due to their size, nanoparticles remain suspended via Brownian motion, avoiding significant phase separation. The low concentration of particles, typically below 5%, ensures that the fluid's flow characteristics are dominated by the base fluid. The nanoparticles enhance thermal properties without significantly affecting flow dynamics. Additionally, the inertia and buoyancy effects of the nanoparticles are negligible, allowing the nanofluid to be treated as a continuous medium,

similar to conventional single-phase fluids, despite the presence of solid particles. The single-phase assumptions for nanofluids have been validated by Xuan and Li [34] and Pak and Cho [35]. Rostamani et al. [36] also applied the single-phase model in their numerical analysis of Al_2O_3 and other nanofluids. The nanofluid is assumed to be incompressible, with turbulent flow characteristics. Furthermore, it is presumed that the liquid and solid particles are in thermal equilibrium and exhibit zero relative velocity.

2.2. Nanofluid Thermophysical Properties

Nanofluid properties are crucial to the advancement of this study. The thermophysical parameters of nanofluids, such as thermal conductivity (k), density (ρ), specific heat (Cp), and viscosity (μ) for different volume fractions (φ), can be estimated using a number of models and correlations. Table 1 represents the thermophysical properties of Al_2O_3 nanoparticles and water at 293 k temperature [37–39].

Table 1. Properties of the base fluid and Al_2O_3 nanoparticle.

Material	ρ [kg/m^3]	Cp [J/kgK]	μ [kg/ms]	k [W/mk]
Water, ϕ = 0%	998.2	4182	9.98×10^{-4}	0.597
Alumina (Al_2O_3)	3880	773	-	36

For this study, the fluid is considered incompressible, and density is considered temperature independent.

Table 2 shows the thermophysical properties of different volume concentrations of the nanofluid at 293 k temperature [40].

Table 2. Thermophysical properties of Al_2O_3 nanofluid.

Fluid	ρ (kg/m^3)	Cp (J/kgK)	μ (kg/ms)	k (W/mk)
1% Al_2O_3	1027.01	4053.21	0.001023	0.62
2% Al_2O_3	1055.83	3931.45	0.001048	0.643
3% Al_2O_3	1084.65	3816.16	0.001073	0.667
4% Al_2O_3	1113.47	3706.84	0.001098	0.692

2.3. Geometry

A square-shaped 3D geometry containing 4 rods (2 × 2 array) has been created using SpaceClaim 2022R1, as shown in Figure 2, to study their thermohydraulic behavior with the Al_2O_3/water nanofluid. The fuel rod bundles are parallel to the flow path of the fluid in a pressurized water reactor, and the unit channel is referred to as the subchannel. Flow symmetry is used to model the single subchannel, which has been extensively modeled before by Ahmed et al. [41]; Nazififard et al. [42]; Nazififard et al. [43]; Liu and Ferng, [44]; and Nematollahi and Nazifi [45].

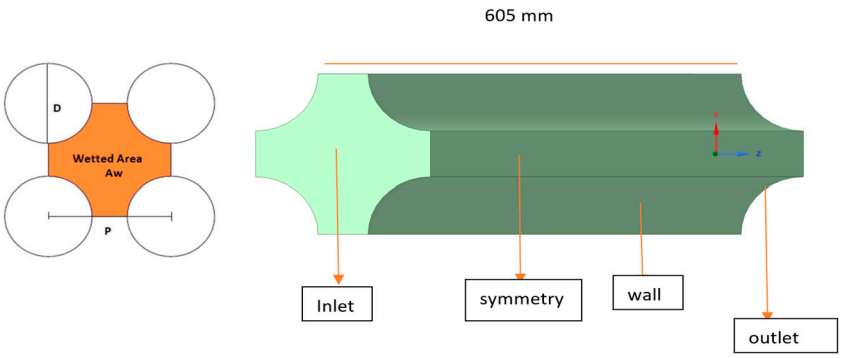

Figure 2. Subchannel geometry.

Table 3 shows the dimensions of the geometry, where the length refers to the distance between the inlet and the outlet of the subchannel, and the pitch is the distance between the centers of two adjacent fuel pins. The diameter (D) represents the fuel rod's width, while the pitch–diameter ratio (P/D) defines the relationship between the pitch and diameter. Additionally, the hydraulic diameter (Dh) is an equivalent diameter used in fluid dynamics for non-circular channels, calculated as Dh = 4 A/P, where A is the cross-sectional flow area, and P is the wetted perimeter of the cross-section.

Table 3. Dimensions of the geometry.

Characteristics	2 × 2 Square Subchannel Dimensions Ahmed et al. [41]
Length (mm)	605
Pitch (mm)	12.75
D (mm)	9.1
P/D	1.401
Dh (mm)	0.0136

The flow duration can be calculated, shown in Table 4, using the following equation given by Häfeli [46]:

$$Z_L = 4.4 \times Re^{1/6}$$

$$L_e = Z_L \times D_h$$

where Z_L is the entry length number, and L_e is the length for fully developed flow and D_h = hydraulic diameter. The length of the subchannel is sufficiently higher than the entrance length to allow the turbulent flow to fully develop. The chosen Reynolds numbers (20,000, 40,000, 60,000, and 80,000) represent the turbulent flow regimes typically observed in high-performance cooling applications, such as heat exchangers, automotive cooling systems, and HVAC systems. These Re values allow for the study of nanofluid performance under realistic industrial conditions where turbulent flows enhance convective heat transfer. The range of Re also helps assess how varying velocities affect both heat transfer efficiency and pressure drop, crucial for optimizing energy use and cooling effectiveness. This selection reflects the balance between maximizing heat dissipation and managing the associated pumping power requirements.

Table 4. Entrance length for full development of turbulent flow.

Re	Entrance Length for Fully Developed Flow (m)
20,000	0.312798
40,000	0.351104
60,000	0.375651
80,000	0.394101

2.4. Governing Equations of Fluid Flow

2.4.1. Continuity Equation (Conservation of Mass)

The continuity equation ensures that mass is conserved in the flow field. This equation states that the net flow of fluid into a volume equals the net flow out, ensuring mass conservation.

$$\frac{\partial p}{\partial t} + \nabla \cdot (\rho v) = 0$$

ρ = fluid density;
v = velocity vector;
t = time;
$\nabla \cdot (\rho v)$ = divergence of mass flux.

For incompressible flow, the density remains constant, leading to the simplified continuity equation:

$$\nabla \cdot (v) = 0$$

2.4.2. Momentum Equation (Navier–Stokes Equation)

The momentum equation, also known as the Navier–Stokes equation, describes how the velocity field evolves over time due to various forces acting on the fluid. This equation captures the balance of forces acting on the fluid, including inertial forces, pressure forces, viscous forces, and external forces.

$$\rho\left(\frac{\partial v}{\partial t} + v \cdot rv\right) = -\nabla p + \mu\nabla^2 v + f$$

μ = dynamic viscosity;
∇p = pressure gradient;
$\nabla^2 v$ = Laplacian of velocity (viscous term);
f = external body force (e.g., gravity).

2.4.3. Energy Equation (Conservation of Energy)

The Energy Equation in CFD, derived from the First Law of Thermodynamics, accounts for the energy changes in a control volume due to heat, work, and changes in internal, kinetic, and potential energy.

$$\rho l\frac{\partial}{\partial t} + v \cdot \vartheta = -\nabla \cdot q + \varphi$$

e = internal energy per unit mass;
q = heat flux;
φ = viscous dissipation.

2.5. Mesh Generation and Numerical Modelling

The commercial modeling software Ansys SpaceClaim was used to generate the mesh. Bianco et al. [37] used Ansys Fluent to numerically model water–Al_2O_3 nanofluid with good accuracy. Following this approach, Fluent [47] was used to conduct the numerical analysis in this study. It is a widely used tool for fluent simulation.

Ahmed et al. [41] explored the thermohydraulic performance of water nanofluids in hexagonal rod bundle subchannels using a polyhedral mesh, which proved highly accurate in capturing complex flow characteristics. They compared various mesh types and found the polyhedral mesh particularly effective due to its ability to conform closely to intricate geometries, enhancing simulation fidelity and reducing numerical diffusion. Building on their work, we adopted a similar geometric configuration in our study, also employing a polyhedral mesh to model the subchannels. This choice, validated by Ahmed et al.'s findings, ensures that our simulations achieve the same level of precision in representing the nuanced flow dynamics within these complex structures. The 3D polyhedral mesh, shown in Figure 3, was generated using fluid meshing with a maximum cell length of 0.00183144 m. At the velocity inlet and pressure outlet, a local mesh size of 0.00059 m has been used (growth rate 1.2). Surface meshes are generated with a minimum mesh size of 0.00059 m and a maximum mesh size of 0.015125 m. Five boundary layers were applied at a growth rate of 1.2 to solve the near-wall regions. Further details on mesh quality have been provided in Appendix A.

The geometry consists of only fluid regions without any voids. To balance simplicity with computational efficiency, a complete volume mesh consisting of 261,199 nodes was selected for the simulations. This choice effectively reduces computational effort while maintaining high mesh quality. The mesh achieved an average orthogonal quality of 0.9647 and an average skewness of 0.0353, both nearing the ideal values of 1 and 0,

respectively, indicating a well-constructed mesh. Figure 4 presents the outcomes corresponding to various node counts, showing that the selected mesh provides the closest match to the correlation, ensuring reliable and accurate simulation results without excessive computational demands.

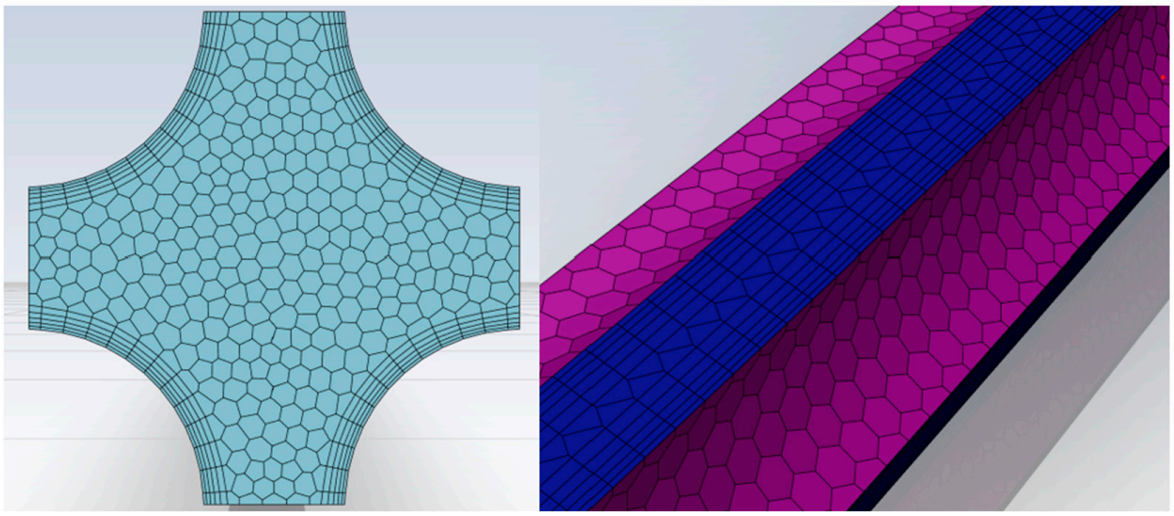

Figure 3. Mesh on the computational domain.

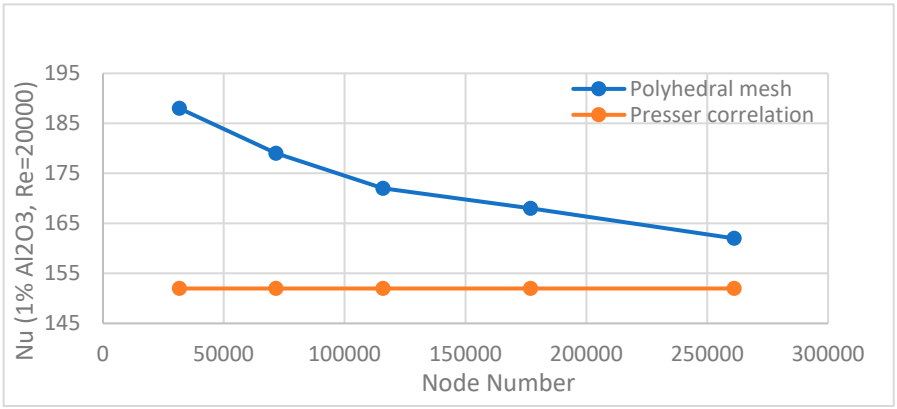

Figure 4. Mesh sensitivity test for different node numbers.

For k-epsilon turbulent models with standard wall treatment, the preferable range of y+ value is 30–300. The target y+ value for this study is kept at around 30.

$$y+ = \frac{\text{density} * \text{velocity} * \text{first layer thickness}}{\text{viscosity}}$$

Inlet velocity (Table 5) has been calculated for different Reynolds numbers ranging from 20,000 to 80,000 using the following equation:

$$\text{Re} = \frac{\rho v D_h}{\mu}$$

where ρ (kg/m^3) is the density of the fluid, v is the inlet velocity, and μ (kg/ms) is the viscosity of the fluid. D_h is the hydraulic diameter of the computational domain.

Table 5. Inlet velocity (m/s).

	Re = 20,000	Re = 40,000	Re = 60,000	Re = 80,000
Water	1.465	2.931	4.396	5.862
1% Al_2O_3	1.46	2.92	4.38	5.84
2% Al_2O_3	1.455	2.91	4.365	5.819
3% Al_2O_3	1.45	2.9	4.35	5.8
4% Al_2O_3	1.445	2.891	4.336	5.781

Turbulent intensity, given in Table 6, for fully developed pipe flow has been estimated using the following equation [33]:

$$I = 0.16 \times Re^{1/8}$$

Table 6. Turbulence intensity.

Re	Turbulence Intensity
20,000	0.046397142
40,000	0.042546367
60,000	0.040443718
80,000	0.039015191

A uniform heat flux (q″) of 50 KW/m^2 has been specified at the wall (rod surface) boundary condition [41]. A no-slip condition has been considered for the fuel rod surface. Zero-gauge pressure has been implemented at the outlet boundary condition. For their study, a comparative study between the RNG k-epsilon and k-omega SST has been carried out and the results support the k-epsilon model as shown in Table 7. The study uses the SIMPLE method to couple pressure and velocity, a widely used approach in fluid flow simulations to ensure stable results. For turbulence parameters, a first-order upwind method is chosen to maintain stability, especially in turbulent flows, by preventing fluctuations in the simulation. For energy and momentum parameters, a second-order upwind method is applied, which improves accuracy by minimizing numerical diffusion—a common source of error in lower-order methods. This higher-order approach allows for a more detailed and accurate representation of the fluid's behavior, especially in areas where the flow changes rapidly. Overall, the combination of these methods ensures that the simulations are both stable and precise.

Table 7. Comparison of turbulence models.

Turbulence Model	Nusselt Number	
	Ahmed et al. [41]	Dittus–Boelter [48] Correlation
Spalart–Allmaras	138	
RNG k-ε	145	144
SST k-ω	157	
Reynold stress model	144	

2.6. Validation of Nusselt Number

The y+ based heat transfer coefficient from FLUENT has been used to calculate the Nusselt number. It has been compared with the established correlations such as Maïga et al. [32], Pak and Cho [35], Notter and Sleicher [49], and Presser [50] to validate the model (Figure 5). Nusselt number has been calculated using the following equation:

$$\text{Nusselt Number (Nu)} = \frac{\text{Heat transfer coefficient(h)} * \text{Hydraulic diameter(Dh)}}{\text{Thermal conductivity of the fluid(K)}}$$

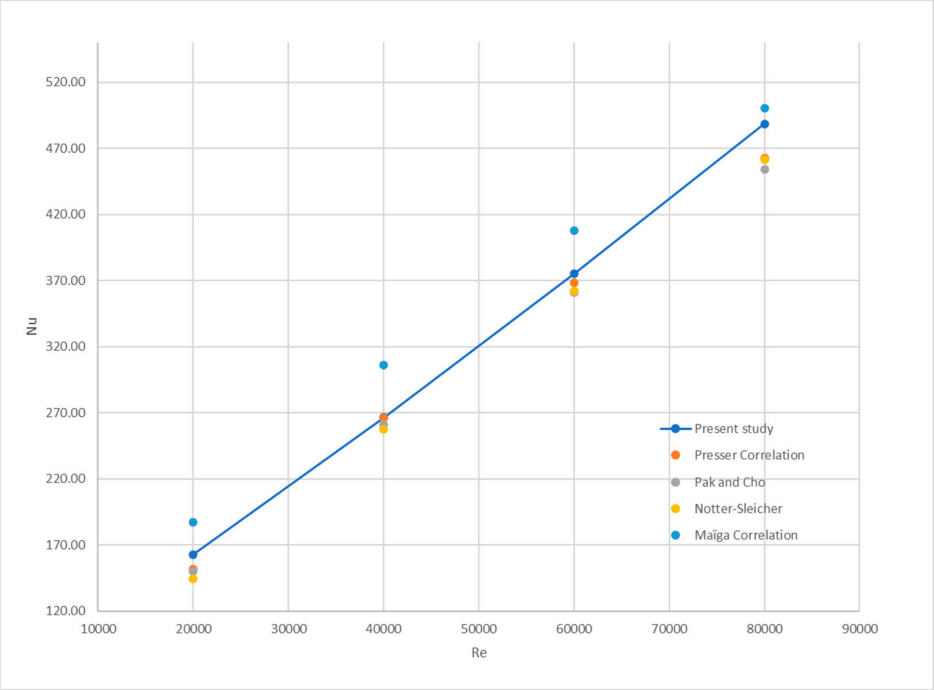

Figure 5. Nusselt number validation by comparing with correlations (1% Al_2O_3).

The established correlations that have been used in this study to verify the results and validate their authenticity are as follows:

Dittus–Boelter [48] correlation: $Nu = 0.023 * Re^{0.8} * Pr^{0.4}$;

Presser [50] correlation: $Nu = \psi * (0.023 * Re^{0.8} * Pr^{0.4})$
where $\psi = 0.9217 + 0.147 * P/D - 0.1130e^{-7(P/D-1)}$;

Notter and Sleicher [49] correlation: $Nu = 5 + (0.015 * (Re^{0.856}) * (Pr^{0.347})$
(Re ranging from 10^4 to 10^6; Pr ranging from 0.1 to 10^4; φ ranging from −10% to 10%);

Pak and Cho [35] correlation: $Nu = 0.021 * Re^{0.8} * Pr^{0.5}$
(Re ranging from 10^4 to 10^5; Pr ranging from 6.5 to 12.3; φ ranging from 0% to 3%);

Maïga et al. [32] correlation: $Nu= 0.085 * Re^{0.71} * Pr^{0.35}$
(Re ranging from 10^4 to 5×10^5; Pr ranging from 6.6 to 13.9; φ ranging from 0% to 10%).

Table 8 gives the Prandtl number, calculated using the following equation:

$$Pr = \frac{\text{Specific Heat Capacity, C} \times \text{DynamicViscosity, } \eta}{\text{Thermal conductivity, k}}$$

Table 8. Prandtl numbers for different volume fractions of nanofluids.

Material	Prandtl Number, Pr
Water	6.9910
1% Al_2O_3	6.6878
2% Al_2O_3	6.4077
3% Al_2O_3	6.1390
4% Al_2O_3	5.8817

3. Results

The results have been presented in terms of convective heat transfer coefficient (h) and Nusselt number (Nu) with respect to variable inlet velocity (Re = 20,000, 40,000, 60,000, and 80,000) and nanofluid concentrations (ϕ ranging from 0% to 4%).

3.1. Impacts of Inlet Velocity

It is observed that the highest Reynold number exhibits the highest heat transfer coefficient (HTC) and Nusselt number across all the volume concentrations (Tables 9 and 10; Figures 6 and 7). As the Reynolds number increases, flow transitions from laminar to turbulent. Turbulent flow involves chaotic fluid motion, enhancing fluid mixing. This brings the bulk fluid closer to heated or cooled surfaces, improving heat transfer through convection. The thinner thermal boundary layer at the wall results in a higher temperature gradient, enhancing the heat transfer coefficient (HTC). As the following data show, HTC goes from 7308.51 to 21,737.37 ~200% (for 0% conc.) as the Re number increases from 20 k to 80 k.

Table 9. Heat transfer coefficients.

		Heat Transfer Coefficients for Different Volume Fractions of Al_2O_3 Nanofluid (W/m^2K)				
		0%	**1%**	**2%**	**3%**	**4%**
Re=	20,000	7308.51	7396.47	7648.06	7819.84	7995.346
	40,000	11,839.76	12,106.36	12,373.15	12,643.14	12,921.74
	60,000	16,865.13	17,046.89	17,626.48	18,010.98	18,405.32
	80,000	21,737.37	22,193.83	22,712.93	23,211.88	23,719.74

Table 10. Nusselt numbers.

		Nusselt Number for Different Volume Fractions of Al_2O_3 Nanofluid				
		0%	**1%**	**2%**	**3%**	**4%**
Re=	20,000	167.04	162.78	162.29	159.97	157.65
	40,000	270.60	266.44	262.56	258.64	254.79
	60,000	385.46	375.17	374.04	368.45	362.91
	80,000	496.82	488.44	481.98	474.85	467.69

The Nusselt number (Nu) is directly proportional to the heat transfer coefficient (HTC). As turbulent mixing increases the HTC, it also leads to a higher Nu. Empirical correlations often express Nu in terms of Reynolds number (Re) and Prandtl number (Pr), as given by the relationship Nu = C * Reˆm * Prˆn. Typically, the exponent 'm' is positive, indicating that as Re increases, Nu also increases.

Different volume concentrations in a fluid impact its viscosity, density, and specific heat capacity. These properties, in turn, influence the Reynolds number and heat transfer characteristics. Generally, as the Reynolds number increases, both the heat transfer coefficient (HTC) and Nusselt number tend to increase. This trend holds true across various volume concentrations, assuming that the fluid properties remain relatively constant. The dominant mechanism for enhanced convective heat transfer in turbulent flow is responsible for this behavior.

In summary, higher Reynolds numbers lead to greater HTC and Nusselt numbers due to improved fluid mixing, reduced boundary layer thickness, and increased temperature gradients near the surface.

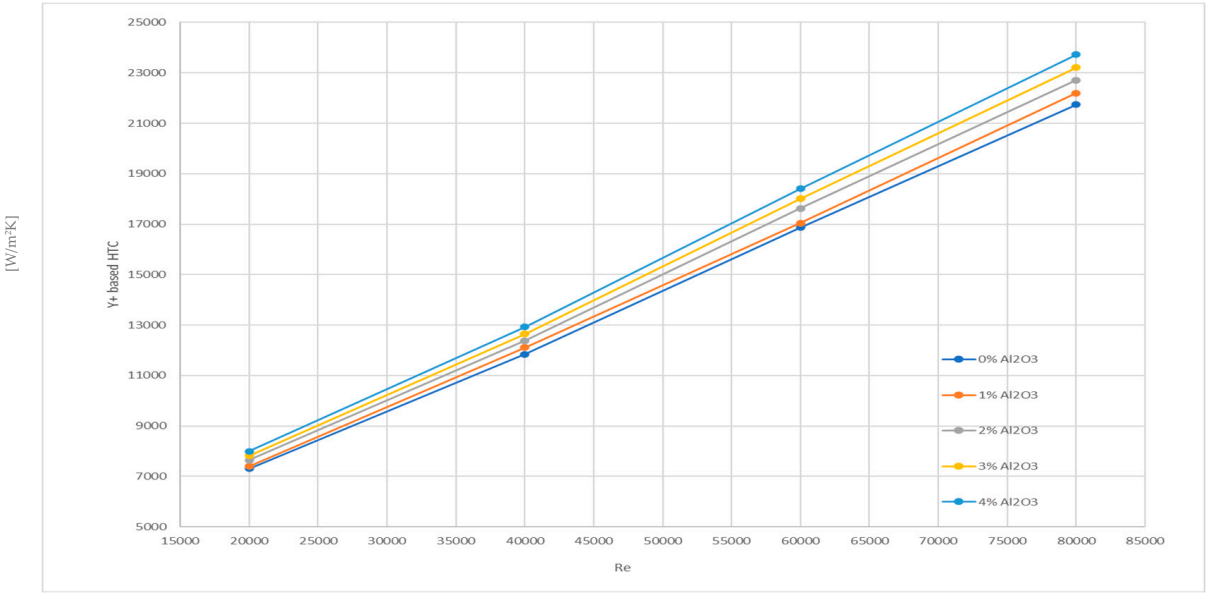

Figure 6. Heat transfer coefficient plot against Reynolds number.

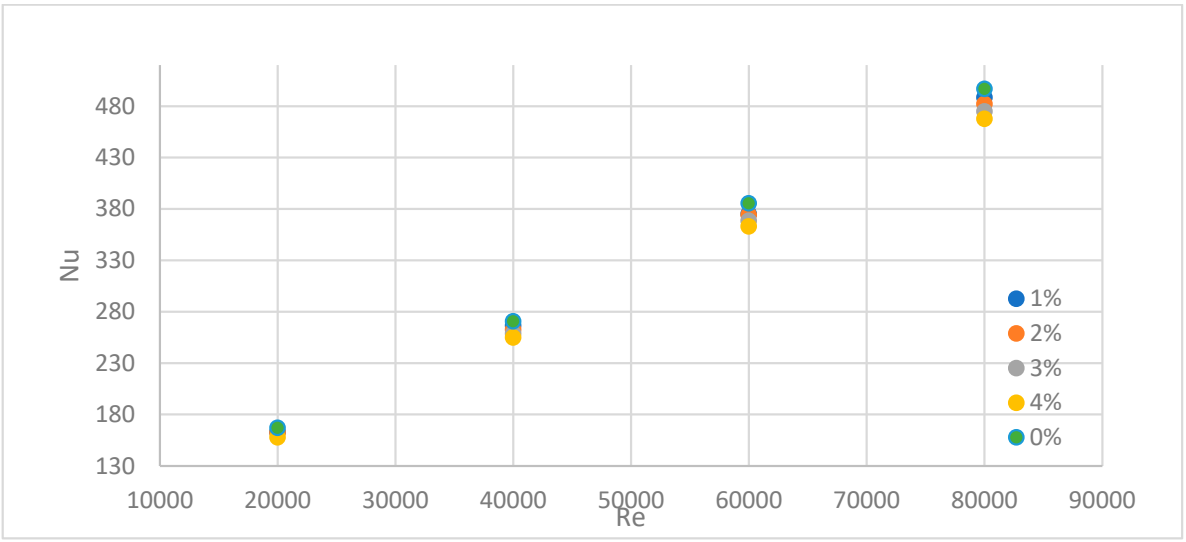

Figure 7. Nusselt number plot against Reynolds number for ϕ = (0% to 4%).

3.2. Impacts of Nanofluid Concentrations

The increase in the heat transfer coefficient (HTC) with the rising volume concentration of nanofluids at a fixed Reynolds number is primarily due to the enhanced thermal properties imparted by the nanoparticles. Nanoparticles increase the effective thermal conductivity of the fluid, facilitate greater surface area for heat transfer, and contribute to better mixing through Brownian motion, all of which enhance the convective heat transfer process. Even though higher concentrations may increase viscosity, the overall effect of improved thermal conductivity and heat capacity leads to a more efficient heat transfer, resulting in a higher HTC. This effect is demonstrated by the simulation results presented in Figure 8 below where the x-axis represents the volume concentration (%) of aluminum oxide and the y-axis represents the HTC.

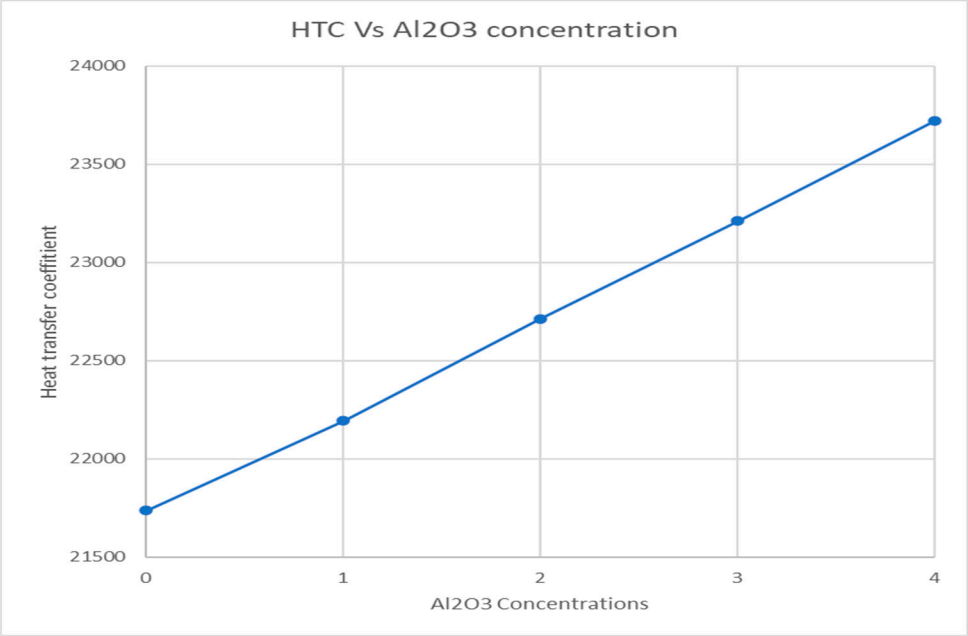

Figure 8. Effects of nanoparticle concentrations on HTC at fixed Re = 80,000.

3.3. Heat Transfer Enhancement Ratio for Nanofluids

The Heat Transfer Enhancement Ratio (HTER) for nanofluids is a measure of the improvement in heat transfer performance due to the addition of nanoparticles. Increasing nanoparticle concentration in the base fluid enhances thermal conductivity, facilitating more efficient heat dispersion and significantly boosting the heat transfer coefficient. This improvement is quantifiable through HTER, which compares the heat transfer coefficients of the base fluid and the nanofluid.

However, an increased nanoparticle concentration inversely affects the Nusselt number, a dimensionless parameter representing the ratio of convective to conductive heat transfer. As thermal conductivity rises, the temperature gradient necessary for convection diminishes, reducing the Nusselt number (Tables 11–14). This inverse relationship suggests that while nanofluids improve the overall heat transfer, the efficiency of convective heat transfer decreases relative to conductive transfer.

Table 11. HTC and Nu enhancement ratio for Re = 20,000.

Vol %	h (Y+ Based)	h(nf)/h(bf)	Nu	Nu(nf)/Nu(bf)
base fluid	7308.52	1.00	167.04	1.00
1	7396.47	1.01	162.78	0.97
2	7648.06	1.05	162.29	0.97
3	7819.85	1.07	159.97	0.96
4	7995.35	1.09	157.65	0.94

Table 12. HTC and Nu enhancement ratio for Re = 40,000.

Vol %	h (Y+ Based)	h(nf)/h(bf)	Nu	Nu(nf)/Nu(bf)
base fluid	11,839.76	1.00	270.60	1.00
1	12,106.36	1.02	266.44	0.98
2	12,373.15	1.05	262.56	0.97
3	12,643.14	1.07	258.64	0.96
4	12,921.74	1.09	254.79	0.94

Table 13. HTC and Nu enhancement ratio for Re = 60,000.

Vol %	h (Y+ Based)	h(nf)/h(bf)	Nu	Nu(nf)/Nu(bf)
base fluid	16,865.13	1.00	385.46	1.00
1	17,046.89	1.01	375.17	0.97
2	17,626.48	1.05	374.04	0.97
3	18,010.98	1.07	368.45	0.96
4	18,405.32	1.09	362.91	0.94

Table 14. HTC and Nu enhancement ratio for Re = 80,000.

Vol %	h (Y+ Based)	h(nf)/h(bf)	Nu	Nu(nf)/Nu(bf)
0 (bf)	21,737.37	1.00	496.82	1.00
1	22,193.83	1.02	488.44	0.98
2	22,712.93	1.04	481.98	0.97
3	23,211.88	1.07	474.85	0.96
4	23,719.74	1.09	467.69	0.94

This dynamic highlights the complexity of optimizing nanofluids for heat transfer applications. While higher thermal conductivity is beneficial, the reduced convective efficiency must be considered. Engineers must balance these factors, ensuring that the enhancement in heat transfer is achieved without compromising the system's overall efficiency, particularly in applications where convective heat transfer is predominant. This careful consideration is crucial for maximizing the effectiveness of heat transfer systems using nanofluids.

3.4. Comparison with Established Correlations

The study compared the Nusselt number for various Al_2O_3 nanofluid volume concentrations (0%, 1%, 2%, 3%, and 4%) with the established correlations to validate the simulation results obtained using FLUENT 2022R1. Figures 9–13 illustrate that the FLUENT results align closely with those predicted by these correlations. For the base fluid (0% Al_2O_3), the Nusselt number versus Reynolds number (Nu vs. Re) plot was compared with the Pak and Cho [35] correlation, showing minimal deviation at a Reynolds number of 40,000. Similarly, the 1% Al_2O_3 concentration was evaluated against both the Presser and Pak and Cho correlations, with the least deviation also occurring at 40,000 Re. For the 3% Al_2O_3 concentration, the comparison with the Pak and Cho [35] and Notter-Sleicher [49] correlations indicated minimum deviation at the same Reynolds number. Lastly, the 4% Al_2O_3 concentration's Nu vs. Re plot was compared with the Notter–Sleicher [49] correlation, again showing the smallest deviation at 40,000 Re. Notably, the maximum deviation for all the volume concentrations was observed at a Reynolds number of 80,000. This higher deviation at 80,000 Re could be attributed to the increased turbulence and complexity in fluid dynamics at higher flow rates, which may not be as accurately captured by the correlations or the simulation model. These consistent findings across different concentrations underscore the reliability of the FLUENT simulations and their close agreement with the established theoretical models.

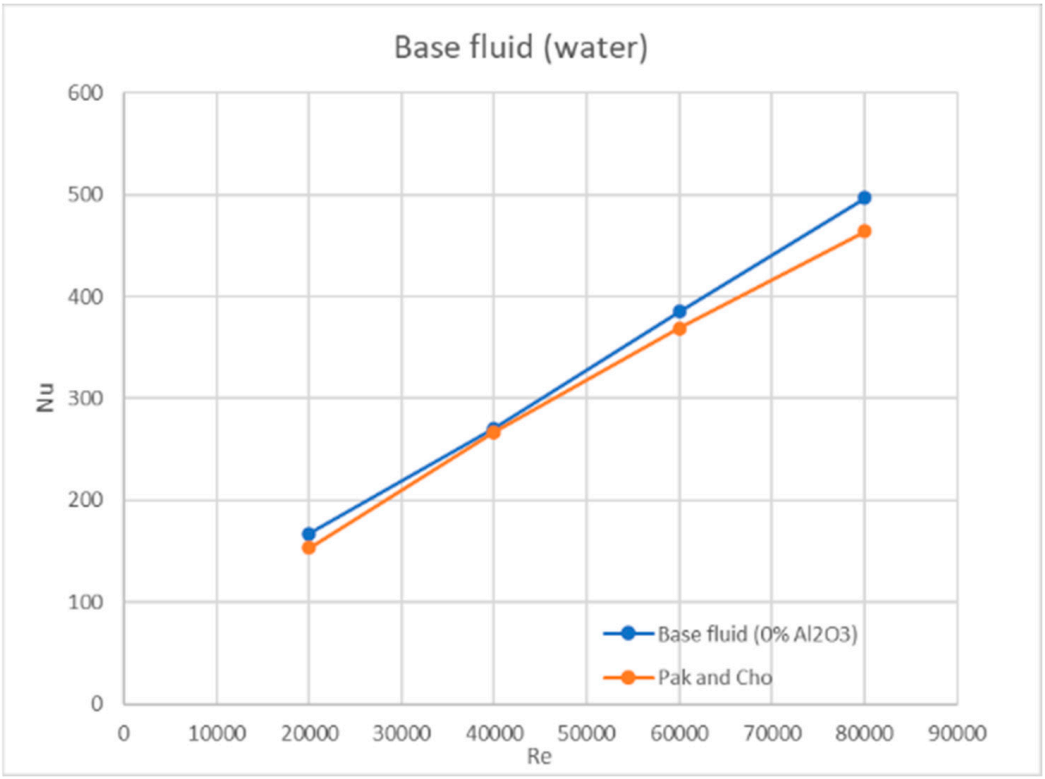

Figure 9. The 0% Al_2O_3 Nu vs. Re plot.

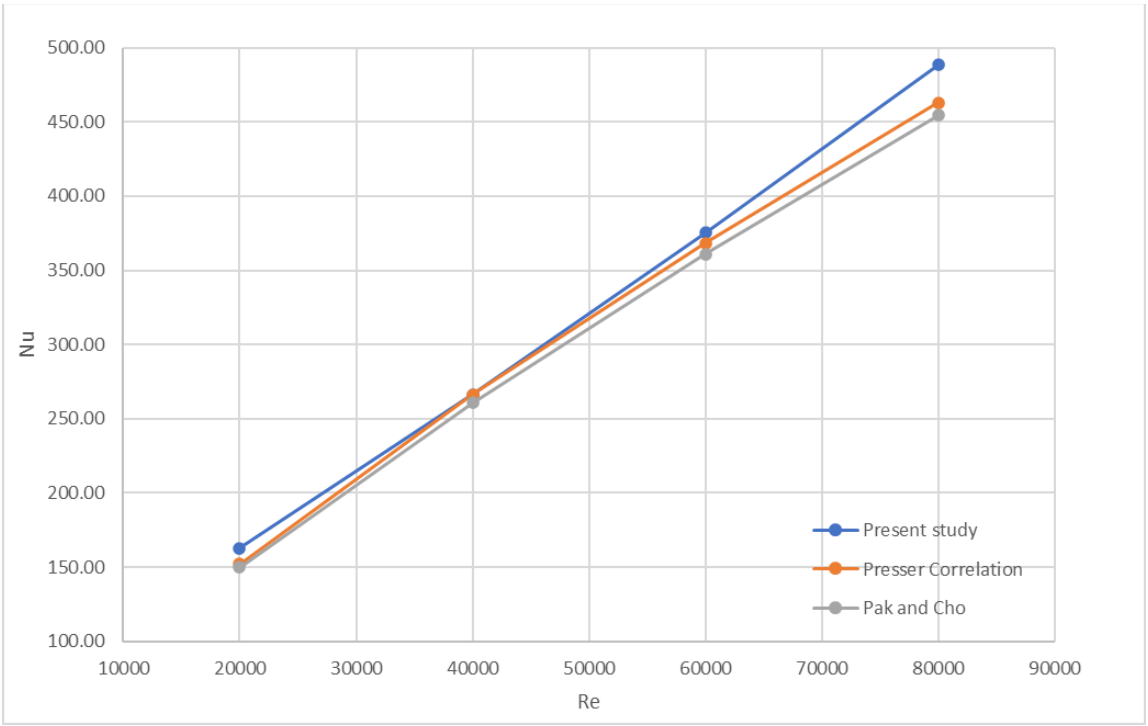

Figure 10. The 1% Al_2O_3 Nu vs. Re plot.

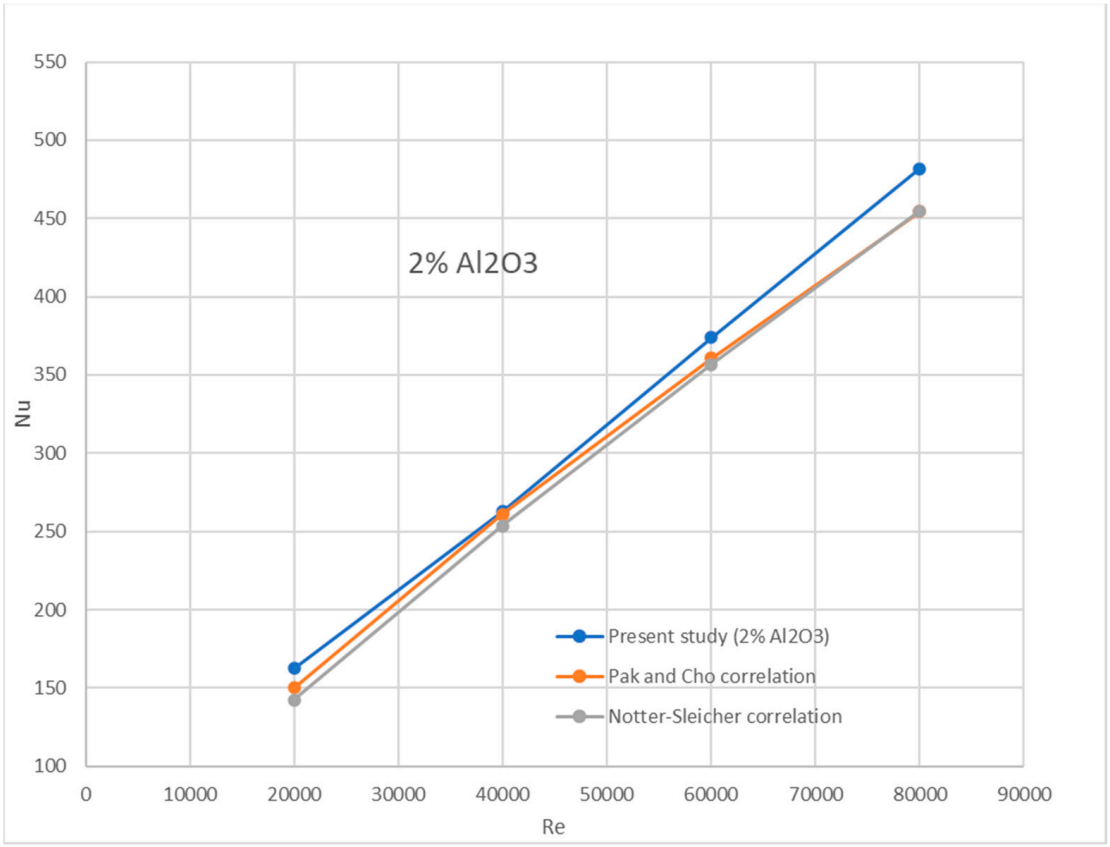

Figure 11. The 2% Al_2O_3 Nu vs. Re plot.

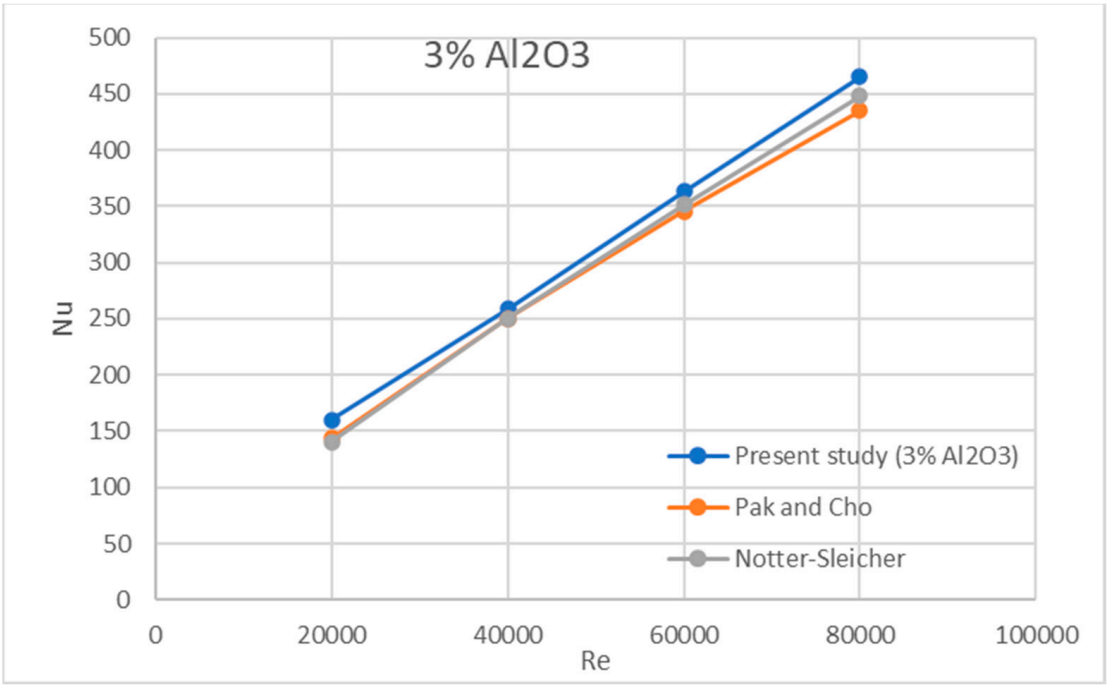

Figure 12. The 3% Al_2O_3 Nu vs. Re plot.

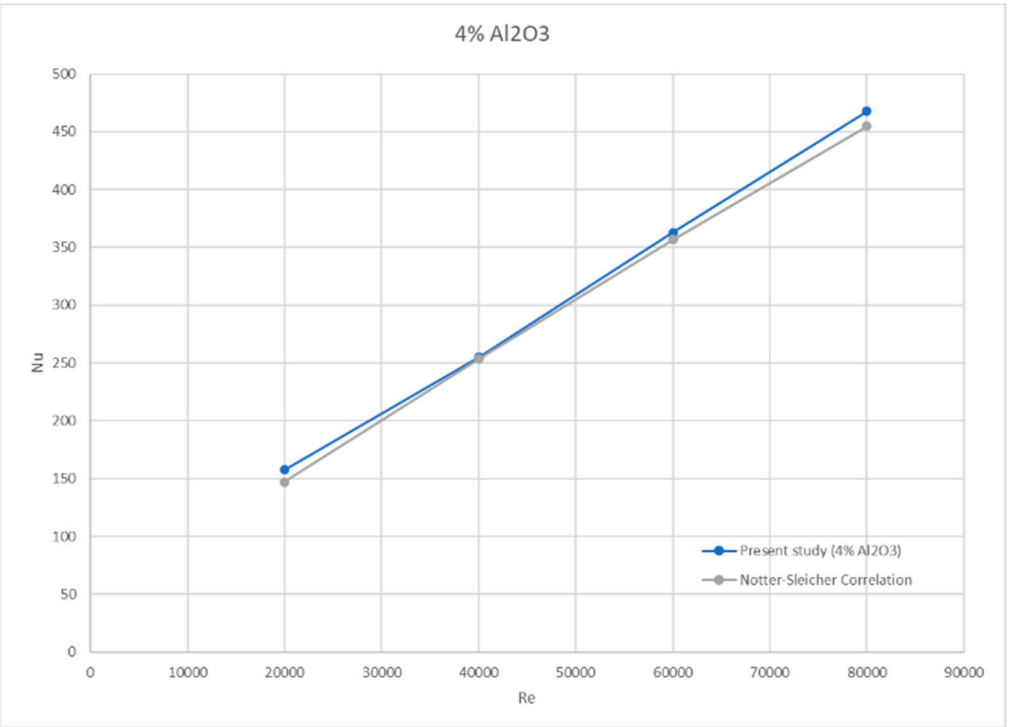

Figure 13. The 4% Al_2O_3 Nu vs. Re plot.

3.5. Flow Characteristics of Different Concentrations of Nanofluid

Very little impact is observed on the velocity profile when nanoparticles are added to the base fluid. When nanoparticles are added to a base fluid, their impact on the velocity profile is generally minimal. This is primarily due to the low volume fraction of the nanoparticles typically used in nanofluids. Despite altering the fluid's density and viscosity slightly, the small size and well-dispersed nature of nanoparticles mean that they do not significantly disturb the flow. As a result, the dominant properties influencing the flow—such as the base fluid's viscosity and density—remain largely unchanged. Consequently, the overall velocity profile experiences minimal alterations. Notably, nanoparticles primarily enhance the thermal properties rather than affecting the momentum-related properties, which explains their negligible impact on the velocity profiles as shown in Figure 14.

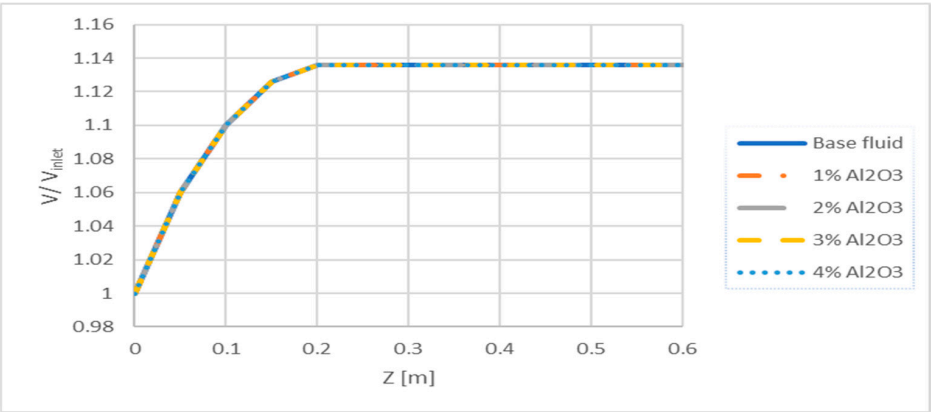

Figure 14. Normalized velocity profile for ϕ = 0%, 1%, 2%, 3%, and 4% at Re = 40,000.

4. Conclusions and Discussion

The study on modeling nanofluids using the k-epsilon turbulence model highlights its effectiveness in enhancing heat transfer performance. A key finding is that nanofluids

significantly improve the heat transfer coefficient of the base fluid, increasing it by a factor of up to 1.09 as both the velocity and nanofluid concentrations rise. This improvement is crucial for applications requiring efficient heat dissipation. However, an intriguing observation is that increasing nanofluid concentration tends to decrease the Nusselt number at a fixed Reynolds number, suggesting a complex interaction between concentration and thermal dynamics. The study also confirms that heat transfer efficiency is positively correlated with higher nanofluid velocity or Reynolds number, emphasizing the potential for optimizing flow conditions to maximize heat transfer. Additionally, the accuracy of the simulation results is validated by their close alignment with the established correlations, with the Dittus–Boelter correlation showing the highest error margin at 15%, while the Presser correlation shows the lowest error margin, ranging between 0 and 7%. Specifically, for a Reynolds number of 80,000, Maïga et al.'s [32] correlation demonstrates a minimal error of 2.42%, reinforcing the reliability of the simulation approach. The findings also indicate that nanofluid concentration has a minimal impact on the fluid velocity profile, suggesting that other factors may play a larger role in determining flow characteristics.

This study provides valuable insights into the field of heat transfer enhancement in nuclear reactor systems through several significant findings:

- Practical Application of Nanofluids in PWRs: The research offers critical insights into the use of Al_2O_3 nanofluids as a coolant in pressurized water reactors (PWRs). The study demonstrates that nanofluids can enhance heat transfer under varying flow conditions, suggesting improvements in thermal management that could lead to safer and more efficient reactor operation by preventing overheating during critical conditions. This has important implications for reactor safety and the potential to extend reactor life without altering fuel assembly design.
- Optimization of Nanofluid Concentrations: The study explores the balance between improving heat transfer and managing the trade-offs, such as increased viscosity and reduced convective efficiency. By providing detailed data on the effect of nanoparticle concentration on the heat transfer coefficient and Nusselt number, this research helps optimize nanofluid concentrations for maximum thermal performance without compromising pumping efficiency. This is particularly relevant for industries focused on energy efficiency and cost savings.
- Contribution to CFD Modeling of Nanofluids: The validation of CFD results through multiple correlations enhances the scientific understanding of nanofluid behavior under turbulent flow conditions. The strong agreement between simulation results and empirical correlations supports the use of CFD to predict nanofluid performance in complex reactor environments, providing a cost-effective alternative to experimental methods.

In conclusion, this study advances the understanding of nanofluid applications in high-performance cooling systems, such as PWRs, and offers actionable insights for improving reactor safety and thermal efficiency.

5. Future Work

Building on these conclusions, future research should deepen the understanding of nanofluids in heat transfer applications. One critical area for exploration is the calculation of pressure drop across nanofluids, which was not addressed in the current study. This analysis could provide valuable insights into the trade-offs between enhanced heat transfer and increased pressure requirements.

An important challenge in nanofluid research is the complex interplay between nanoparticle concentrations, sizes, and base fluid properties. Nanoparticles can alter the thermal conductivity and viscosity of the base fluid, yet their impact on heat transfer is not always linear or straightforward. For instance, while a higher concentration of nanoparticles generally improves thermal conductivity, it may also increase fluid viscosity, leading to a potential decrease in convective heat transfer if the flow becomes significantly more resistive. Additionally, the distribution and dispersion of nanoparticles within the

fluid can affect heat transfer efficiency; the agglomeration or sedimentation of nanoparticles may lead to non-uniform properties, impacting performance.

Another challenge lies in accurately modeling the thermal and hydrodynamic behavior of nanofluids. The k-epsilon turbulence model, while effective, may not fully capture the complexities introduced by nanoparticles, such as the effects of Brownian motion or enhanced heat conduction at the nanoparticle–fluid interface. More sophisticated models, including those that account for the micro-scale interactions between nanoparticles and the fluid, could provide deeper insights.

Future studies should also explore the impact of different nanoparticle materials and geometries on heat transfer performance. For example, the thermal properties and stability of various nanoparticle types—such as metals, oxides, or carbon-based materials—could reveal new avenues for optimizing nanofluids for specific applications. Furthermore, investigating the heat transfer performance in non-ideal or extreme conditions, such as high temperatures or varying pressures, could extend the applicability of nanofluids in diverse engineering scenarios.

Finally, exploring novel experimental techniques and advanced simulation methods will be crucial for validating theoretical models and enhancing the practical understanding of nanofluids. Addressing these challenges will not only improve the efficiency of heat transfer systems but also expand the potential applications of nanofluids in advanced thermal management technologies.

Author Contributions: Methodology, M.A.I.S. and M.R.; Software, M.A.I.S. and M.R.; Validation, M.A.I.S.; Resources, M.A.I.S.; Data curation, M.A.I.S.; Writing—original draft, M.A.I.S.; Writing—review & editing, M.A.I.S. and M.R.; Supervision, P.R. All authors have read and agreed to the published version of the manuscript.

Funding: This research received no external funding.

Data Availability Statement: The original contributions presented in the study are included in the article, further inquiries can be directed to the corresponding author.

Acknowledgments: We extend our heartfelt thanks to Philip Rubini at the University of Hull for his invaluable support and guidance throughout this study. We are also deeply grateful to the University of Hull for granting access to its chemistry lab and library computers, and for providing a welcoming and conducive environment for our research.

Conflicts of Interest: The authors declare no conflict of interest.

Appendix A

```
Calculation complete.

          Area-Weighted Average
   Yplus Based Heat Tran. Coef.          [W/(m^2 K)]
------------------------------- --------------------
                           wall             23211.878
```

```
Calculation complete.

          Area-Weighted Average
   Yplus Based Heat Tran. Coef.          [W/(m^2 K)]
------------------------------- --------------------
                           wall             18010.975
```

```
Calculation complete.

          Area-Weighted Average
   Yplus Based Heat Tran. Coef.          [W/(m^2 K)]
------------------------------- --------------------
                           wall              12643.14
```

```
Calculation complete.

          Area-Weighted Average
   Yplus Based Heat Tran. Coef.          [W/(m^2 K)]
------------------------------- --------------------
                           wall              7819.849
```

Figure A1. Y+-based HTC from FLUENT for 3% Al_2O_3/water nanofluid for Re = 20 k, 40 k, 60 k, and 80 k.

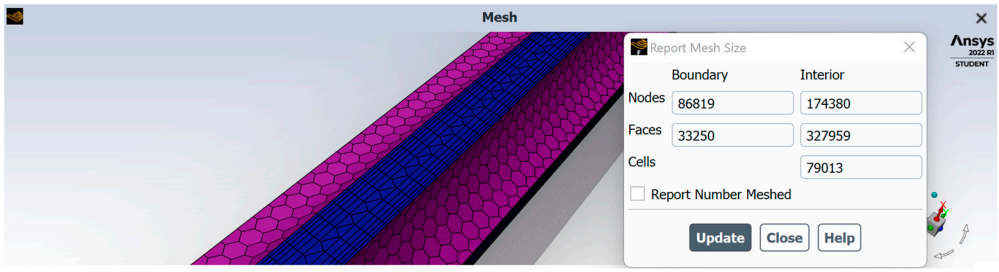

Figure A2. Node, cell, and face numbers.

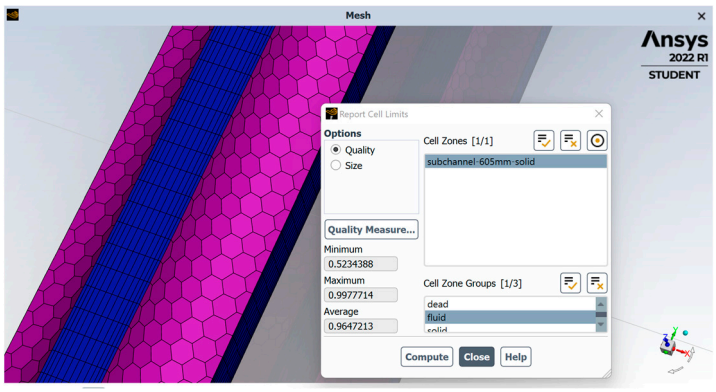

Figure A3. Mesh quality (orthogonal quality).

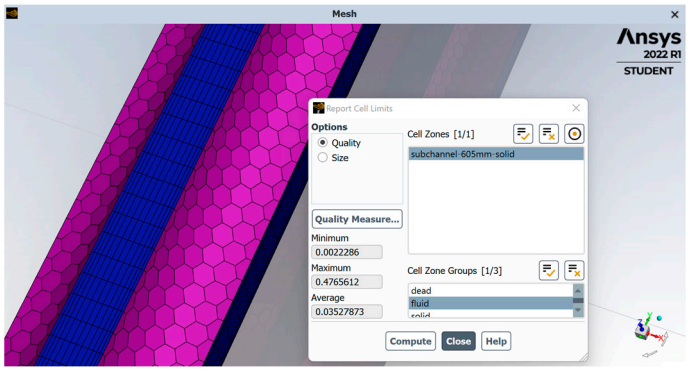

Figure A4. Mesh quality (skewness).

Table A1. Comparison with correlations for 1%volume concentration.

Re	h (Y+ Based)	Present Study	Pak and Cho	Presser Correlation	Dittus and Boelter	Notter-Sleicher	Maiga
20,000	7396.5	162.8	149.9	152.0	141.6	144.4	187.1
40,000	12,106.4	266.4	260.9	266.3	246.6	257.2	306.0
60,000	17,046.9	375.2	360.9	368.4	341.1	361.9	408.1
80,000	22,193.8	488.4	454.3	463.0	429.3	461.6	500.6

Table A2. Comparison with correlations for 2%volume concentration.

Re	h (Y+ Based)	Nu Y+ Based	Pak and Cho	Notter-Sleicher
20,000	7648.1	162.3	149.9	142.3
40,000	12,373.2	262.6	260.9	253.5
60,000	17,626.5	374.0	360.9	356.7
80,000	22,712.9	482.0	454.3	454.8

Table A3. Comparison with correlations for 3%volume concentration.

Re	h (Y+ Based)	Nu Y+ Based	Presser Correlation	Pak and Cho	Notter-Sleicher
20,000	7819.8	160.0	159.9	143.6	140.3
40,000	12,643.1	258.6	258.6	250.0	249.9
60,000	18,011.0	368.4	368.5	345.8	351.5
80,000	23,211.9	474.8	474.9	435.3	448.2

Table A4. Comparison with correlations for 4%volume concentration.

Re	h (Y+ Based)	Nu Y+ Based	Pak and Cho	Notter-Sleicher
20,000	7995.3	157.7	140.5	138.3
40,000	12,921.7	254.7	244.7	246.3
60,000	18,405.0	362.9	338.4	346.4
80,000	23,719.0	467.7	426.0	441.7

References

1. Fenech, H. *Heat Transfer and Fluid Flow in Nuclear Systems*; Elsevier: Amsterdam, The Netherlands, 2013.
2. Končar, B.; Krepper, E.; Bestion, D.; Song, C.-H.; Hassan, Y.A. Two-Phase Flow Heat Transfer in Nuclear Reactor Systems. *Sci. Technol. Nucl. Install.* **2013**, *2013*, 587839. [CrossRef]
3. Das, S.K. Heat and Mass Transfer Issues Associated with Nuclear Reactor Safety. *Heat Transf. Eng.* **2015**, *36*, 857–858. [CrossRef]
4. Oka, Y. *Nuclear Reactor Design*; Springer: Berlin/Heidelberg, Germany, 2014.
5. Yoon, S.J.; Kim, S.B.; Park, G.C.; Yoon, Y.H.; Cho, H.K. Application of CUPID for subchannel-scale thermal–hydraulic analysis of pressurized water reactor core under single-phase conditions. *Nucl. Eng. Technol.* **2018**, *50*, 54–67. [CrossRef]
6. Bhowmik, P.K.; Shamim, J.A.; Chen, X.; Suh, K.Y. Rod bundle thermal-hydraulics experiment with water and water-Al_2O_3 nanofluid for small modular reactor. *Ann. Nucl. Energy* **2021**, *150*, 107870. [CrossRef]
7. Saha, S.; Khan, J.; Farouk, T. Numerical study of evaporation assisted hybrid cooling for thermal powerplant application. *Appl. Therm. Eng.* **2020**, *166*, 114677. [CrossRef]
8. Tusar, M.; Ahmed, K.; Bhuiya, M.; Bhowmik, P.; Rasul, M.; Ashwath, N. CFD study of heat transfer enhancement and fluid flow characteristics of laminar flow through tube with helical screw tape insert. *Energy Procedia* **2019**, *160*, 699–706. [CrossRef]
9. Manglik, R.M. Heat transfer enhancement. In *Heat Transfer Handbook*; John Wiley & Sons: Hoboken, NJ, USA, 2003; pp. 1029–1130.
10. Choi, S.U.; Eastman, J.A. *Enhancing Thermal Conductivity of Fluids with Nanoparticles*; ANL: Argonne, IL, USA, 1995.
11. Bejan, A.; Kraus, A.D. *Heat Transfer Handbook*; John Wiley & Sons: Hoboken, NJ, USA, 2003.
12. Xuan, Y.; Li, Q. Heat transfer enhancement of nanofluids. *Int. J. Heat Fluid Flow* **2000**, *21*, 58–64. [CrossRef]
13. Koo, J.; Kleinstreuer, C. Impact analysis of nanoparticle motion mechanisms on the thermal conductivity of nanofluids. *Int. Commun. Heat Mass Transf.* **2005**, *32*, 1111–1118. [CrossRef]
14. Keblinski, P.; Phillpot, S.; Choi, S.U.; Eastman, J. Mechanisms of heat flow in suspensions of nano-sized particles (nanofluids). *Int. J. Heat Mass Transf.* **2002**, *45*, 855–863. [CrossRef]
15. Buongiorno, J. Convective Transport in Nanofluids. *J. Heat Transfer.* **2006**, *128*, 240–250. [CrossRef]
16. Darvanjooghi, M.H.K.; Esfahany, M.N. Experimental investigation of the effect of nanoparticle size on thermal conductivity of in-situ prepared silica–ethanol nanofluid. *Int. Commun. Heat Mass Transf.* **2016**, *77*, 148–154. [CrossRef]
17. Saidur, R.; Leong, K.Y.; Mohammed, H.A. A review on applications and challenges of nanofluids. *Renew. Sustain. Energy Rev.* **2011**, *15*, 1646–1668. [CrossRef]
18. Kumar, D. Hybrid Nanofluids: Preparation, Characterization, and Applications. *J. Nanotechnol.* **2018**, *81*, 1669–1689.
19. Nobrega, G.; de Souza, R.R.; Gonçalves, I.M.; Moita, A.S.; Ribeiro, J.E.; Lima, R.A. Recent Developments on the Thermal Properties, Stability and Applications of Nanofluids in Machining, Solar Energy and Biomedicine. *Appl. Sci.* **2022**, *12*, 1115. [CrossRef]
20. Oyeleke, O.; Ohunakin, O.; Adelekan, D.; Atiba, O.; Nkiko, M.; Jatinder, G. Recent Advancements in the Development of Nanofluid Technology in Heat Transfer Applications. *IOP Conf. Ser. Mater. Sci. Eng.* **2021**, *1107*, 012209. [CrossRef]
21. Khalid, R.Z.; Iqbal, M.; Hassan, A.; Haris, S.M.; Ullah, A. Improved Heat Transfer Capabilities of Nanofluids—An Assessment Through CFD Analysis. *Chem. Eng. Technol.* **2024**, *47*, e202300523. [CrossRef]
22. Uzun, S. Investigation of the Thermal Effects of MgO and ZnO Nanoparticles in a Pressurized Water Reactor Coolant with Computational Fluid Dynamics Model. *Nucl. Technol.* **2024**, 1–13. [CrossRef]
23. Ponkty, M.; Puja, A.; Mollah, A.S. Numerical Investigation of Nanofluid's Heat Transfer Performance in Passive Residual Heat Removing System of AP1000 Nuclear Reactor. *WSEAS Trans. Adv. Eng. Educ.* **2024**, *21*, 80–91. [CrossRef]
24. Khouri, O.; Goshayeshi, H.R.; Mousavi, S.B.; Hosseini Nami, S.; Zeinali Heris, S. Heat transfer enhancement in industrial heat exchangers using graphene oxide nanofluids. *ACS Omega* **2024**, *9*, 24025–24038. [CrossRef]

25. Zhuang, X.; Xie, Y.; Li, X.; Yue, S.; Wang, H.; Wang, H.; Yu, P. Experimental investigation on flow boiling of HFE-7100 in a microchannel with pin fin array. *Appl. Therm. Eng.* **2023**, *225*, 120180. [CrossRef]
26. Ghafouri, A.; Toghraie, D. Experimental study on thermal conductivity of SiC-ZnO/ethylene glycol hybrid nanofluid: Proposing an optimized multivariate correlation. *J. Taiwan Inst. Chem. Eng.* **2023**, *148*, 104824. [CrossRef]
27. Marseglia, G.; De Giorgi, M.; Pontes, P.; Solipa, R.; Souza, R.; Moreira, A.; Moita, A. Enhancement of microchannel heat sink heat transfer: Comparison between different heat transfer enhancement strategies. *Exp. Therm. Fluid Sci.* **2024**, *150*, 111052. [CrossRef]
28. Shojib, S.I.; Sardar, M.A.I.; Joarder, S.A.; Zakir, G.; Hossain, A. Heat Transfer Analysis of Nanofluid Based Coolant Used in the Sub-Channel of Fuel Assembly of a Pressurized Water Reactor. *J. Nanofluids* **2023**, *12*, 580–588. [CrossRef]
29. Khashaei, A.; Ameri, M.; Azizifar, S. Heat transfer enhancement and pressure drop performance of Al_2O_3 nanofluid in a laminar flow tube with deep dimples under constant heat flux: An experimental approach. *Int. J. Thermofluids* **2024**, *24*, 100827. [CrossRef]
30. Alshukri, M.J.; Hamad, R.F.; Eidan, A.A.; Al-Manea, A. Convective Heat Transfer Analysis in Turbulent Nanofluid Flow Through a Rectangular Channel with Staggered Obstacles: A Numerical Simulation. *Int. J. Thermofluids* **2024**, *23*, 100753. [CrossRef]
31. Nazififard, M.; Nematollahi, M.; Jafarpour, K.; Suh, K.Y. Augmented safety heat transport in research reactor IR-40 using nanofluid. *Atw. Int. Z. Fuer Kernenerg.* **2012**, *57*, 262–270.
32. Maïga, S.E.B.; Nguyen, C.T.; Galanis, N.; Roy, G.; Maré, T.; Coqueux, M. Heat transfer enhancement in turbulent tube flow using Al_2O_3 nanoparticle suspension. *Int. J. Numer. Methods Heat Fluid Flow* **2006**, *16*, 275–292. [CrossRef]
33. Ansys. Ansys Fluent. 2022. Available online: https://www.ansys.com/webinars/ansys-fluent-update (accessed on 12 August 2022).
34. Xuan, Y.; Li, Q.; Hu, W. Aggregation structure and thermal conductivity of nanofluids. *AIChE J.* **2003**, *49*, 1038–1043. [CrossRef]
35. Pak, B.C.; Cho, Y.I. Hydrodynamic and heat transfer study of dispersed fluids with submicron metallic oxide particles. *Exp. Heat Transf.* **1998**, *11*, 151–170. [CrossRef]
36. Rostamani, M.; Hosseinizadeh, S.; Gorji, M.; Khodadadi, J. Numerical study of turbulent forced convection flow of nanofluids in a long horizontal duct considering variable properties. *Int. Commun. Heat Mass Transf.* **2010**, *37*, 1426–1431. [CrossRef]
37. Bianco, V.; Chiacchio, F.; Manca, O.; Nardini, S. Numerical investigation of nanofluids forced convection in circular tubes. *Appl. Therm. Eng.* **2009**, *29*, 3632–3642. [CrossRef]
38. Bianco, V.; Nardini, S.; Manca, O. Enhancement of heat transfer and entropy generation analysis of nanofluids turbulent convection flow in square section tubes. *Nanoscale Res. Lett.* **2011**, *6*, 252. [CrossRef] [PubMed]
39. Rohsenow, W.M.; Hartnett, J.R. *Handbook of Heat Transfer*; Choice Rev. Online; McGraw-Hill: New York, NY, USA, 1999; Volume 36, pp. 3336–3347.
40. Gupta, S.; Singh, J.; Gill, B.K. Numerical and CFD analysis of a heat transfer enhancement in turbulent flow through a circular pipe using nanofluid. IOP Conference Series. *Mater. Sci. Eng.* **2022**, *1225*, 12021. [CrossRef]
41. Ahmed, F.; Abir, M.A.; Bhowmik, P.K.; Deshpande, V.; Mollah, A.S. Thermohydraulic performance of water mixed Al_2O_3, TiO_2 and graphene-oxide nanoparticles for nuclear fuel triangular subchannel. *Therm. Sci. Eng. Prog.* **2021**, *24*, 100929. [CrossRef]
42. Nazififard, M.; Nematollahi, M.; Suh, K.Y. Numerical Analysis of Water-Based Nanofluid Coolant for Small Modular Reactor. In Proceedings of the ASME 2011 Small Modular Reactors Symposium, Washington, DC, USA, 28–30 September 2011; pp. 199–205.
43. Nazififard, M.; Nematollahi, M.; Jafarpur, K.; Suh, K.Y. Computational analysis for research reactor IR-40 rod bundle. *Atw. Int. Z. Fuer Kernenerg.* **2012**, *57*, 523–529.
44. Liu, C.C.; Ferng, Y.M. Numerically simulating the thermal–hydraulic characteristics within the fuel rod bundle using CFD methodology. *Nucl. Eng. Des.* **2010**, *240*, 3078–3086. [CrossRef]
45. Nematollahi, M.R.; Nazifi, M. Enhancement of heat transfer in a typical pressurized water reactor by different mixing vanes on spacer grids. *Energy Convers. Manag.* **2008**, *49*, 1981–1988. [CrossRef]
46. Häfeli, R. Fluid Dynamic Characterization of Single-and Multiphase Flow in Structured Porous Media. Master's Thesis, ETH-Zürich, Zürich, Switzerland, 2010.
47. Fluent Inc. *FLUENT 6.3 User's Guide*; Fluent Inc.: Canonsburg, PA, USA, 2006.
48. Dittus, F.W.; Boelter, L.M.K. Heat transfer in automobile radiators of the tubular type. *Int. Commun. Heat Mass Transf.* **1985**, *12*, 3–22. [CrossRef]
49. Notter, R.; Sleicher, C. A solution to the turbulent Graetz problem—III Fully developed and entry region heat transfer rates. *Chem. Eng. Sci.* **1972**, *27*, 2073–2093. [CrossRef]
50. Presser, K. *Heat Transfer and Pressure Loss of Reactor Fuel Elements in the Form of Longitudinal Flow Through Round Rod Bundles*; Institut fuer Reaktorbauelemente: Juelich, Germany, 1967.